

Article

Fe(III) Precipitation and Copper Loss from Sulphate-Chloride Solutions at 150 °C: A Statistical Approach

Tasawar Javed and Edouard Asselin * 

Department of Materials Engineering, The University of British Columbia, 309-6350 Stores Road, Vancouver, BC V6T 1Z4, Canada; tasawarj@interchange.ubc.ca

* Correspondence: edouard.asselin@ubc.ca; Tel.: +1-604-822-1918

Received: 28 April 2020; Accepted: 17 May 2020; Published: 20 May 2020



Abstract: The purification of hydrometallurgical process solutions by Fe(III) precipitation is a common and large-scale industrial operation. This step is notorious for valuable metal loss occurring with the iron precipitation product, which is usually directed to tailings. In this study, factors affecting Fe(III) precipitation and associated copper loss were studied in synthetic process solutions using statistical methods. The variables studied were: Initial acid concentration, retention time, seed addition, and initial Fe(III), Cu(II), and chloride concentrations. The importance of each variable and its interaction effects were studied against two responses, i.e., percent of Fe(III) precipitated as hematite and percent of Cu lost to solids. The results showed that a combination of high acid and moderate seeding was required to simultaneously achieve high proportions of Fe(III) precipitated as hematite and lower copper loss to the precipitates. High acid concentrations create low supersaturation for Fe(III), which minimizes the consequences of homogeneous nucleation and favors particle growth.

Keywords: hematite precipitation; copper loss; supersaturation; pressure leaching; statistical analysis

1. Introduction

Pressure leaching of sulphide concentrates has emerged as an alternative to roasting or a way to increase the capacity of a hydrometallurgical plant without increasing sulphuric acid production [1]. During pressure oxidation, sulphide minerals are oxidized to convert valuable metals into their acid soluble forms. Equation (1) describes a general reaction during the pressure oxidation of chalcopyrite at 150 °C. Leaching at this temperature is often referred to as “medium-temperature leaching”. This classification results from the properties of sulphur: Between 119.3 and 159 °C sulphur is molten and highly fluid; however, above 159 °C it becomes highly viscous [2]. Oxidation of sulphides under medium-temperature conditions leads primarily to an elemental sulphur product rather than sulphate (which requires neutralization). Thus, the primary objective of medium-temperature pressure oxidation is to maximize metal extraction while minimizing sulphur oxidation [1].



Iron precipitation is an important integral step of this process, in particular, but it also remains one of the biggest challenges in the development of sustainable extractive metallurgy, in general. The precipitation of iron, as shown in Equation (1), is much more complicated than indicated by the reaction stoichiometry. Early-stage attempts to remove iron from medium-temperature leach liquors resulted in poorly crystalline and gelatinous precipitates [3]. Over time, and mostly through the development of the electrolytic zinc industry, four iron removal processes were industrialized: The jarosite process, the goethite process, the paragoethite process, and the hematite process [4].

Each process is named according to the major iron phase precipitated. However, all the iron in the process solution is not precipitated as intended. Ferrihydrite ($\text{Fe}^{3+} + 6\text{H}_2\text{O} \rightarrow 5\text{Fe}_2\text{O}_3 \cdot 9\text{H}_2\text{O} + 3\text{H}^+$) is considered to be the first product of Fe(III) hydrolysis and it is a precursor for stable iron oxides such as goethite and hematite [5]. Transformation to crystalline products proceeds via two competing mechanisms: (1) Hematite nucleates and grows within the solid precursor by dehydration and an internal rearrangement process and (2) the formation of goethite involves dissolution of iron from ferrihydrite followed by re-precipitation of the crystalline oxide in solution. Which mechanism predominates depends on a number of factors such as acid levels, temperature, retention time, and the presence of seed [6]. Transformation kinetics are usually slow. Das et al. [7] confirmed that only 50% of ferrihydrite was transformed to hematite and/or goethite after 9 h at 100 °C and a pH of ~2.0. Zic et al. [8] also observed slow transformation of ferrihydrite at 160 °C. If the transformation process does not go to completion, a substantial amount of poorly crystalline or X-ray amorphous phase will exist in the residue [9–11]. Recent studies have identified significant proportions of ferrihydrite and other iron oxyhydroxides in hydrometallurgical residues [9–16]. Precipitation of ferrihydrite or other poorly crystalline phases causes higher valuable metal loss to the residue, raises environmental stability concerns, and renders the residue difficult to characterize [11]. In the processes where retention time is short, a higher proportion of ferrihydrite or other poorly crystalline phases may exist. In concentrated ferric sulphate solutions, in the pH range ~1–2, a similarly structured schwertmannite is a more common phase than ferrihydrite [17]. Schwertmannite is represented by the ideal formula $\text{Fe}_8\text{O}_8(\text{OH})_6\text{SO}_4$ and is a complex hydroxy ferric sulphate with a poorly crystalline nature. Claassen et al. [18] suggested that schwertmannite and ferrihydrite are similar except for the fact that schwertmannite contains higher sulphate content. However, Loan et al. [19] have said that schwertmannite can be distinguished from ferrihydrite, at least qualitatively, on the basis of its hedgehog morphology.

On the other hand, hematite is thermodynamically more stable and does not adsorb much of the valuable metals and it may have commercial value. The increasing depletion of primary copper ores and increasingly stringent environmental regulations necessitate a minimum loss of valuable metal to the residue and a stable product for disposal. This potential for a reduction in metal loss is an economic incentive to the operators of medium-temperature leach processes to improve the quality of their Fe precipitates.

In the case of chalcopyrite pressure leaching, losses of the valuable metal can be minimized by carefully selecting the right combination of process parameters, and their levels, to make a better-quality residue. Thus, a better understanding of the relative importance of readily controllable process parameters would be useful to reduce the amount of amorphous/ poorly crystalline phase and associated metal loss to the residue. Precipitation of hematite at higher temperature from pure Fe(III) chloride solutions [20,21] and pure Fe(III) sulphate solutions [22–25] has been previously studied. However, there is limited work for mixed sulphate-chloride solutions other than that done by Dutrizac and Chen and a more recent publication from the current authors [24,26]. Thus, for these mixed sulphate-chloride solutions, the effect of process parameters on the extent of hematite precipitation is not well understood. In the current study, a systematic (design of experiments) analysis of the process parameters that affect Fe(III) precipitation, and associated copper loss, from sulphate-chloride solutions under medium-temperature conditions was carried out. The precipitation conditions that maximize the amount of hematite while minimizing copper loss to the precipitating solids were studied.

The range of each factor was selected to simulate the same process conditions encountered in typical CESL (Cominco Engineering Services Limited, a subsidiary of Teck Corporation) and Vale medium-temperature hydrometallurgical processes, i.e., 150 °C and retention time of 1 h. However, the results can be applied to any medium-temperature hydrometallurgical process with similar processing conditions. The CESL process typically operates at shorter retention times (1 h) as it was realized during pilot plant operations that longer retention times result in a minimal increase in copper extraction but more undesirable sulphur and pyrite oxidation [27].

Herein, the relative importance and interaction effects of important variables were studied using statistical design of experiments [28,29]. In the preliminary experiments (“initial screening”), the effect of each factor was studied by changing one factor at a time while keeping all others constant. The important factors, identified by this one-variable approach, were then screened using one-quarter fractional factorial design [30]. Significant factors and their interaction effects from fractional factorial design were further identified using a Box-Behnken design [31]. This experimental strategy was skeptically analyzed by Burkin [32] and has been successfully applied to goethite precipitation by Agatzini and Burkin [33] and iron precipitation from atmospheric nickel sulphate solutions by Wang et al. [29]. Multiple regression analysis of the data was employed to develop a best fit mathematical model.

2. Experimental

Initial solutions were prepared using reagent-grade chemicals ($\text{CuSO}_4 \cdot 5\text{H}_2\text{O}$, $\text{Fe}_2(\text{SO}_4)_3 \cdot 7\text{H}_2\text{O}$, LiCl) and deionized water (10 Mega Ohms). A titanium autoclave from the Parr Instruments company was used for all the experiments. One liter of solution was placed in a two-liter glass liner (24.7 × 9.65 cm) before being transferred to the autoclave. Agitation speed was fixed to 500 rpm. Agitation was provided with the help of two impellers with a 5.7-cm diameter. Lithium chloride was preferred as a source of chloride instead of the more commonly available sodium chloride. The presence of the sodium ion would have resulted in the precipitation of sodium jarosite. Reagent-grade hematite seed with an average particle size of about 18 μm was used in some of the experiments. The particle size distribution of the final product was measured with a Malvern Mastersizer 2000 Laser Diffraction Particle Size Analyzer.

Solutions in the autoclave were heated from room temperature to 150 °C in ~35 min. The autoclave was kept at 150 °C for one hour (or for whichever retention time was tested) and then cooled to room temperature in about five minutes. The autoclave was operated at a steam pressure of 400–500 kilopascals (without overpressure from O_2). At the end of the experiments, i.e., after precipitation at 150 °C for a given retention time, the solids were separated from the solutions using a vacuum filter and Whatman 42 ashless filter paper. The precipitates were then washed with excess amounts of warm deionized water and left to dry overnight in an oven at 60 °C. After drying, the solids were digested and analyzed by Inductively Coupled Plasma-Optical Emission Spectrometry (ICP-OES) (error limit $\pm 6\%$). Aqua regia was used to digest the solid samples before ICP analysis. Chloride analysis of the solids was carried out by digesting in 6% nitric acid followed by silver nitrate titration (detection limit of 0.001%). About 2–3 g of the solids were analyzed by quantitative X-ray powder diffraction (QXRPD). The QXRPD analysis of the solids was done via the Rietveld method using X-ray powder diffraction data. The solid samples were ground to <10 μm before analysis. The quantification of the amorphous phase was done by adding a known amount of an internal standard of corundum, with more details described in [26]. This method measures the amorphous content with an accuracy of about 2% [34]. Continuous-scan X-ray powder-diffraction data were collected over a range of 3–80° 2 θ with Co K α radiation on a Bruker D8 Focus Bragg-Brentano diffractometer. The X-ray diffraction patterns shown in this study are the calculated patterns from the Rietveld refinement analysis. A representative XRD pattern and Rietveld refinement plots are given in Appendix A (Figures A3–A5).

Final free acid concentration of the solutions was measured by titration with 0.1 molar (M) NaOH. A solution of Magnesium-EthyleneDiamineTetraacetic Acid (Mg-EDTA) (0.2 M MgSO_4 + 0.1 M EDTA) was used to complex metal ions that would normally contribute hydrogen ions by hydrolysis [35].

For scanning electron microscopy (SEM), a small amount of the washed and dried sample was suspended in water and a few drops of the mixture were dried on carbon tape before imaging. The images were collected using the secondary electron (SE) mode.

The contour plots presented in this study were obtained using the software package Design-Expert® version 9.0.5.1 (STAT-EASE) and originPro 8SR0 v8.0724 (B724).

3. Initial Screening

Initial screening experiments were carried out to study the effect of initial concentrations of: Ferric ion, H_2SO_4 , retention time, chloride ion, cupric ion, and reagent-grade hematite seed. The effect of each variable was recorded against two responses, i.e., percent of Fe(III) (%Fe(III)) precipitated as hematite and percent of Cu(II) loss to solids. Most of the experiments were carried out over the base conditions: 6 g/L Fe(III), 11 g/L Cl^- , 30 g/L Cu(II), and 15 g/L H_2SO_4 for 1 h at 150 °C. The variables and their ranges that produced the maximum amount of hematite are given in Table 1 while plots for individual variable responses are given in Appendix A, Figures A1 and A2. A brief summary of initial screening experiments is given below.

Table 1. Variables and their ranges used for the factorial design experiments. Hematite was the dominant precipitate within these ranges.

Factor	Variable	Low Level (–)	High Level (+)	Units
A	Initial Fe(III)	6	15	g/L
B	Initial H_2SO_4	0	15	g/L
C	Retention time	1	6	h
D	Initial chloride	0	30	g/L
E	Hematite seed	0	15	g/L

Results of the screening experiments showed that %Fe(III) precipitation increased as the initial H_2SO_4 concentration decreased from 25 to 0 g/L. However, due to an increase in the equilibrium ferric concentration of the solution at higher acidities, negligible amounts of iron were precipitated when the initial H_2SO_4 concentration of the solution was >25 g/L. XRD analysis of the precipitates showed them to consist mostly of hematite, except in the absence of hematite seed and acid, where small amounts of goethite were precipitated along with hematite.

Higher initial ferric levels (>15 g/L Fe(III)) reduced %Fe(III) precipitation to a significant extent because of slower precipitation kinetics. XRD analysis of the precipitates showed them to consist of predominantly poorly crystalline hematite at lower ferric concentrations (<15 g/L Fe(III)), see Appendix A, Figure A3 XRD plot. At higher ferric concentrations (>15 g/L Fe(III)) hydronium jarosite was kinetically favored (see XRD, Figure A3 in Appendix A). The raw XRD data used to plot Figure A3 are shown in Figures A4 and A5. Based on these results, a ferric concentration of 6–15 g/L was selected for further investigation. This initial ferric concentration range was close to that of a real leach solution in a medium-temperature pressure oxidation process [36].

Increasing retention times in the system containing 15 g/L H_2SO_4 , 6 g/L Fe(III), 11 g/L Cl^- , and 30 g/L Cu(II) at 150 °C increased the %Fe(III) precipitation. Virtually constant amounts of iron were precipitated for retention times of 6 h and higher. The XRD analysis confirmed the precipitates to consist of predominantly hematite. Therefore, retention times of 1–6 h were selected for further study.

It was found that a small amount of copper was always required for iron precipitation from the system containing initial concentrations of: 15 g/L H_2SO_4 , 6 g/L Fe(III), and 11 g/L Cl^- , for 1 h at 150 °C. Negligible (<5%) iron precipitation occurred in the absence of initially added Cu(II) (as $CuSO_4$). Increasing copper concentration increased the %Fe(III) precipitation and a nearly constant amount of iron was precipitated for copper concentrations of ~30 g/L and higher. The increase in iron precipitation in the presence of $CuSO_4$ was probably due to the formation of bisulphate (HSO_4^-) via the extra sulphate added to the system, which resulted in a decrease in activity of the hydrogen ion. Further discussion on this point can be found in [26]. The XRD analysis of the precipitates showed the precipitates to consist of hematite as the dominant phase irrespective of the copper concentration. Therefore, copper concentration was fixed at 30 g/L for further experiments.

Increasing chloride concentration from 0–30 g/L also increased the %Fe(III) precipitation in the system containing 15 g/L H_2SO_4 , 6 g/L Fe(III), 1 h and 150 °C. XRD analysis of the precipitates showed

a relatively higher amount of hematite for higher chloride concentrations. Chloride concentrations of 0–30 g/L were thus further investigated in the fractional factorial design.

Increasing hematite seed levels from 0–15 g/L also increased the %Fe(III) precipitation but a virtually constant amount of iron precipitation was obtained at higher seed levels. Seed concentrations of 0–15 g/L were then further studied.

Only the conditions that favored hematite precipitation were selected for statistical analysis, “%Fe(III) precipitation” herein refers to “%Fe(III) precipitated as hematite”, even though a certain amount of other phases will necessarily coexist.

4. Fractional Factorial Design

Studying one variable at a time allows for simple interpretation. However, the way each variable is interrelated with another cannot be interpreted through the single-variable technique. The advantage of the fractional factorial technique is the fact that several variables are changed together so that the interaction between variables can be identified using only a small number of experiments.

The significance of the factors and their levels, identified through the screening experiments, was tested by designing a one-quarter fractional factorial design of resolution III. An unreplicated fractional factorial design at two levels, low (–) and high (+), was employed. The levels of the variables are given in Table 1 and the layout of the design is given in Table 2. The selection of the low (–) and high (+) levels of the variables was based on the screening experiments and these represent the ranges of a typical medium-temperature hydrometallurgical process. Because of the short retention times, the final solutions of the precipitation experiments were not always in equilibrium.

Table 2. Screening experiments for fractional factorial design in coded and actual form.

Experiment No.	Variables Studied									
	A		B		C		D		E	
	Coded	Actual	Coded	Actual	Coded	Actual	Coded	Actual	Coded	Actual
F-1	+	15	—	0	—	1	—	0	+	15
F-2	+	15	—	0	+	6	—	0	—	0
F-3	+	15	+	15	—	1	+	30	—	0
F-4	+	15	+	15	+	6	+	30	+	15
F-5	—	6	+	15	—	1	—	0	—	0
F-6	—	6	—	0	+	6	+	30	—	0
F-7	—	6	—	0	—	1	+	30	+	15
F-8	—	6	+	15	+	6	—	0	+	15

Box–Behnken Design

The important variables identified by fractional factorial design and their interaction effects were studied in more detail by using a Box–Behnken design [37]. Details of the Box–Behnken design are given in Appendix B. The factors studied were: Initial H₂SO₄ concentration, initial ferric concentration, and concentration of hematite seed. The factors were studied at three levels low (–), medium (0), and high (+). The factors and their levels are given in Table 3. The Box–Behnken design with three factors and 15 experiments including three central points is given in Table 4.

Table 3. Factors and their ranges used for the Box–Behnken experiments.

Factor	Variable	Low Level (–)	Medium (0)	High Level (+)	Units
A	Initial Fe(III)	6	10.5	15	g/L
B	Initial H ₂ SO ₄	0	7.5	15	g/L
E	Seed	0	7.5	15	g/L

Table 4. Design matrix for Box–Behnken experiments.

Experiment No.	Variables Studied					
	A		B		C	
	Coded	Actual	Coded	Actual	Coded	Actual
G-1	—	6	+	15	0	7.5
G-2	+	15	0	7.5	0	7.5
G-3	—	6	0	7.5	0	7.5
G-4	+	15	+	15	0	7.5
G-5	+	15	—	0	—	0
G-6	0	10.5	+	15	—	0
G-7	0	10.5	0	7.5	—	0
G-8	—	6	—	0	—	0
G-9	—	6	—	0	+	15
G-10	0	10.5	0	7.5	+	15
G-11	0	10.5	+	15	+	15
G-12	+	15	—	0	+	15
G-13	0	10.5	0	7.5	0	7.5
G-14	0	10.5	0	7.5	0	7.5
G-15	0	10.5	0	7.5	0	7.5

5. Results and Discussion

5.1. Fractional Factorial Design

Experimental results of the fractional factorial design are given in Table 5. Because a fractional factorial design does not have enough degrees of freedom, conventional analysis of variance (ANOVA) cannot be used. In this study, data were analyzed by plotting half-normal probability plots for the effect estimates [38]. Half-normal probability plots are recommended for experiments utilizing a small number of tests [31]. These are plots of the absolute value of the effect estimates against their cumulative normal probabilities. It is assumed that only the main factors (i.e., A, B, C, etc.) and their low-order interactions (i.e., two-factor interactions: AB, BC, etc.) are dominant and the higher-order interactions (three factor and higher, i.e., ABC, ABCD, etc.) are negligible. In these graphs, the factors with small and/or insignificant effects fall on a straight line on the plot while factors with comparatively larger and more significant effects visually fall off the straight line. For example, while chloride, factor D, did affect Fe(III) precipitation (Figure A1), the half-normal probability plot in Figure 1 did not reveal this factor to be as important as the others. The presence of chloride in medium-temperature leaching is known to affect the kinetics through processes that are not fully understood [27]; however, it has a negligible effect on metal loss to the precipitates [26]. The effect of chloride on Fe(III) precipitation is believed to be due to the formation of ferric chloride species that may be more mobile and, thus, collide more readily than sulphate complexes. This is discussed in more detail in [26] and in references therein.

Table 5. Elemental analysis of the fractional factorial design experiments.

Experiment No.	Precipitates Fe, S Content (%)		%Fe(III) Precipitated	Cu in Solids (%)
	Fe	S		
F-1	62.3	1.33	57.0	0.16
F-2	59.7	2.57	73.4	0.19
F-3	47.8	5.72	10.2	0.09
F-4	64.0	1.09	48.3	0.08
F-5	56.2	2.47	14.9	0.04
F-6	61.6	1.58	86.6	0.05
F-7	64.5	0.91	94.6	0.04
F-8	66.2	0.62	79.9	0.07

Figures 1 and 2 show half-normal probability graphs for: “%Fe(III) precipitated” and “%Cu content of the precipitates”, respectively. Due to a large variation in the amount of product formed,

the Cu uptake of the product was gauged by %Cu content of the precipitates instead of %Cu loss to the solids. For example, when all other conditions were kept constant, except increasing retention time from 1 h to 6 h, Cu concentration in the precipitates changed only marginally; however, the product yield (P.Y.) or total mass of the precipitates almost tripled for the 6-h retention time. This resulted in higher %Cu loss to solids for the 6-h product; however, %Cu content of the product did not change significantly.

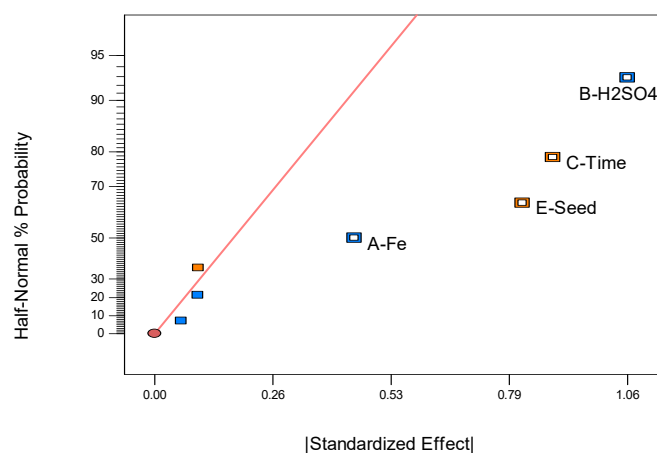


Figure 1. Half-normal probability plot for the factors and their interactions for log (%Fe(III) precipitated).

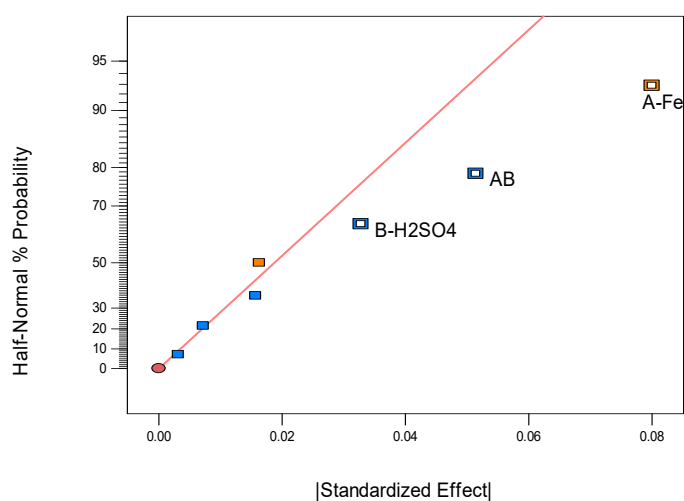


Figure 2. Half-normal probability plot for the factors and their interactions for “%Cu content of the precipitates”.

The data for %Fe(III) precipitation were described by a log transformation (Appendix C), due to large variation in the response values. Such transformations are often used for stabilizing the variance of the response, making the distribution of the response closer to the normal distribution and improving the fit of the model to the data [31]. Details of the procedure have been discussed by Box and Cox [39] and Box et al. [30]. Details of the transformation procedure used in this study is given in Appendix C.

Figure 1 shows that the factors A, B, C, and E have large effects on %Fe(III) precipitation for the system under study, while Figure 2 shows that the factors A, B, and their interaction AB are the most important factors for the copper loss to solids. Factor C, i.e., retention time, showed significance for Fe(III) precipitation (Figure 1). However, it did not show significance for Cu(II) loss to the precipitates (Figure 2), therefore, it was screened out in the interaction effects. The interaction term AB is important because the equilibrium constant for the ferric precipitation, Equation (2), is defined by both terms.



Ferric precipitation involves the nucleation of hematite and subsequent growth of the solid nuclei to larger particles. The agglomeration-growth mechanism depends on the ferric iron supersaturation of the solution where the growth of the particles occurs by the attachment of embryos to the surface of the crystal or by agglomeration of the crystals. Both processes play an important role in defining the copper content and quality of the final product. Higher supersaturation leads to a faster nucleation, which results in small particles, larger surface area, and a relatively higher adsorption of divalent ions [21,23,40]. At lower supersaturation, initially fewer nuclei are created, which further grow to larger particles. In such cases, larger particles and relatively lower adsorption or solution entrapment are achieved [21,23].

Fractional factorial designs usually have low resolution, where the main effects can be differentiated from one another but the main effects cannot be differentiated from some of the low-order interactions (AB, BC, etc.). Further, some of the low order interactions also cannot be differentiated from one another [31]. Therefore, the effects of A, B, C, E, and AB, in Figures 1 and 2, are confounded with BD + CE, AD + CDE, AE + BDE, AC + BCD, and D + BCE, respectively. Higher-order interaction effects are usually negligible in a fractional factorial design, and the system is left with main factors and two-factor interactions only. Although the main factors cannot be differentiated from the two-factor interactions, the factors A and B had a significant effect on “%Cu content” of the solids. Similarly, the factors A, B, C, and E resulted in a wide variation in “%Fe(III) precipitated”. Since longer retention times put economic constraints on hydrometallurgical processes by limiting reactor throughput and since a certain amount of seed is always present in a continuous commercial process, the factors A, B, and E were studied in more detail in a Box–Behnken design.

Variables which might possibly affect the chosen responses, but were fixed throughout the experimental work for Box–Behnken design, were: Retention time, 1 h; temperature, 150 °C; 30 g/L Cu(II); 11 g/L Cl⁻; and agitation speed, 500 rpm.

5.2. Optimization for the Factors

The important factors (A, B, and E) identified by fractional factorial design were further investigated using a Box–Behnken design at three levels with 15 experiments. The factors and their levels are given in Table 3 and the experimental results are given in Table 6.

The method of least squares was applied to the data to fit quadratic models for the “%Fe(III) Precipitated” and “%Cu Content” of the precipitates. The predicted models for the two responses are given in Equations (3) and (4), with the analysis of variance (ANOVA) results in Table 7. The statistical significance of the models was tested by Fisher’s F-test. Normally, p-values of less than 0.05 for significant terms and greater than 0.05 for “lack of fit” are considered good to explain the statistical significance of the model.

$$\begin{aligned} \% \text{Fe(III) Precipitated} = & 101.738 - 3.953 \times [\text{Fe}] - 3.188 \times [\text{H}_2\text{SO}_4] + 1.825 \times [\text{Seed}] + \\ & 0.162 \times [\text{H}_2\text{SO}_4] \times [\text{Seed}] - 0.082 \times [\text{Seed}]^2 \end{aligned} \quad (3)$$

$$\begin{aligned} \% \text{Cu Content} = & 1.292 - 0.086 \times [\text{Fe}] - 0.050 \times [\text{H}_2\text{SO}_4] - 0.070 \times [\text{Seed}] + 0.003 \times [\text{Fe}] \\ & \times [\text{H}_2\text{SO}_4] + 0.002 \times [\text{Fe}]^2 + 0.003 \times [\text{Seed}]^2 \end{aligned} \quad (4)$$

where [Fe], [H₂SO₄], and [Seed] are the initial concentrations of ferric iron, sulphuric acid, and hematite seed, respectively.

It can be seen in Table 7 that significant terms in both the fitted quadratic models have very small p-values, while p-values for “lack of fit” are greater than 0.05 in both the models. The “R-Squared” values, for “%Fe(III) Precipitated” and “%Cu Content” of the solids, were 0.9911 and 0.9729, respectively. For both models, the “Predicted R-Squared” values were in good agreement with the “Adjusted

R-Squared”, i.e., the difference was less than 0.1, demonstrating the statistical significance of the models [41]. The model results were plotted as 2D contour plots as shown in Figures 3 and 4. The results show that the interaction of factors A and B had significant effect on the %Cu content of the precipitates while the interaction of B and E had significant effect on the %Fe(III) precipitated (see Table 7, p -value < 0.05).

Table 6. Compositional analysis of the Box–Behnken design experiments.

Experiment No	Precipitates Fe, S Content (%)		%Fe(III) Precipitated	Cu in Solids (%)
	Fe	S		
G-1	64.6	0.89	60.7	0.03
G-2	63.4	1.36	34.2	0.13
G-3	58.5	1.18	72.5	0.25
G-4	61.2	1.23	22.8	0.05
G-5	48.0	4.04	44.2	0.49
G-6	53.4	2.87	10.0	0.29
G-7	51.8	2.91	39.2	0.52
G-8	54.8	1.98	75.8	0.86
G-9	60.4	0.86	86.6	0.53
G-10	62.6	1.00	65.6	0.15
G-11	63.3	0.95	56.0	0.07
G-12	59.5	1.20	52.0	0.16
G-13	60.5	1.37	54.0	0.12
G-14	60.9	1.39	53.0	0.15
G-15	60.7	1.38	55.0	0.14

Table 7. Analysis of variance for the fitted quadratic models.

Source.	%Fe(III) Precipitated					% Cu Content				
	Sum of Squares	df ¹	Mean Square	F Value	p -Value Prob > F	Sum of Squares	df	Mean Square	F Value	p -Value Prob > F
Model	5578.98	5	1115.80	199.90	<0.0001	0.77	6	0.13	126.66	<0.0001
A-Fe	2531.87	1	2531.87	453.59	<0.0001	0.047	1	0.047	45.74	0.0001
B-H ₂ SO ₄	1512.89	1	1512.89	271.04	<0.0001	0.12	1	0.12	117.56	<0.0001
C-Seed	1366.95	1	1366.95	244.89	<0.0001	0.20	1	0.20	194.17	<0.0001
AB	-	-	-	-	-	0.054	1	0.054	53.48	<0.0001
BC	458.45	1	458.45	82.13	<0.0001	-	-	-	-	-
A ²	-	-	-	-	-	0.006	1	0.006	6.07	0.0391
C ²	67.93	1	67.93	12.17	0.0068	0.11	1	0.11	103.52	<0.0001
Residual	50.24	9	5.58	-	-	0.008	8	1.017 × 10 ⁻³	-	-
Lack of Fit	48.24	7	6.89	6.89	0.1325	0.008	6	1.279 × 10 ⁻³	5.50	0.1617
Pure Error	2.00	2	1.00	-	-	4.647 × 10 ⁻⁴	2	2.323 × 10 ⁻⁴	-	-
Corrected-Total	5629.22	14	-	-	-	0.78	14	-	-	-

¹ degree of freedom.

Figure 3a contour plot shows that in the presence of 15 g/L initially added H₂SO₄, 6 g/L Fe(III), and 0 g/L seed, about 35% of the iron precipitates in 1 h. However, addition of 15 g/L hematite seed under the same conditions increased %Fe(III) precipitation to about 75%. The presence of hematite seed increased the precipitation kinetics (by lowering the critical energy for nucleation). The beneficial effect of hematite seed on precipitation kinetics is discussed in more detail by Dutrizac and Riveros [21] and Dutrizac and Chen [24,25]. Figure 3b,c shows that in the presence of higher amounts of initially added Fe(III), the amount of Fe(III) precipitation again decreased. This decrease was due to the generation of acid by the excess ferric in the system, which in fact increased the equilibrium ferric concentration of the solution. The initial and final free acid concentrations of all experiments are shown in Table 8.

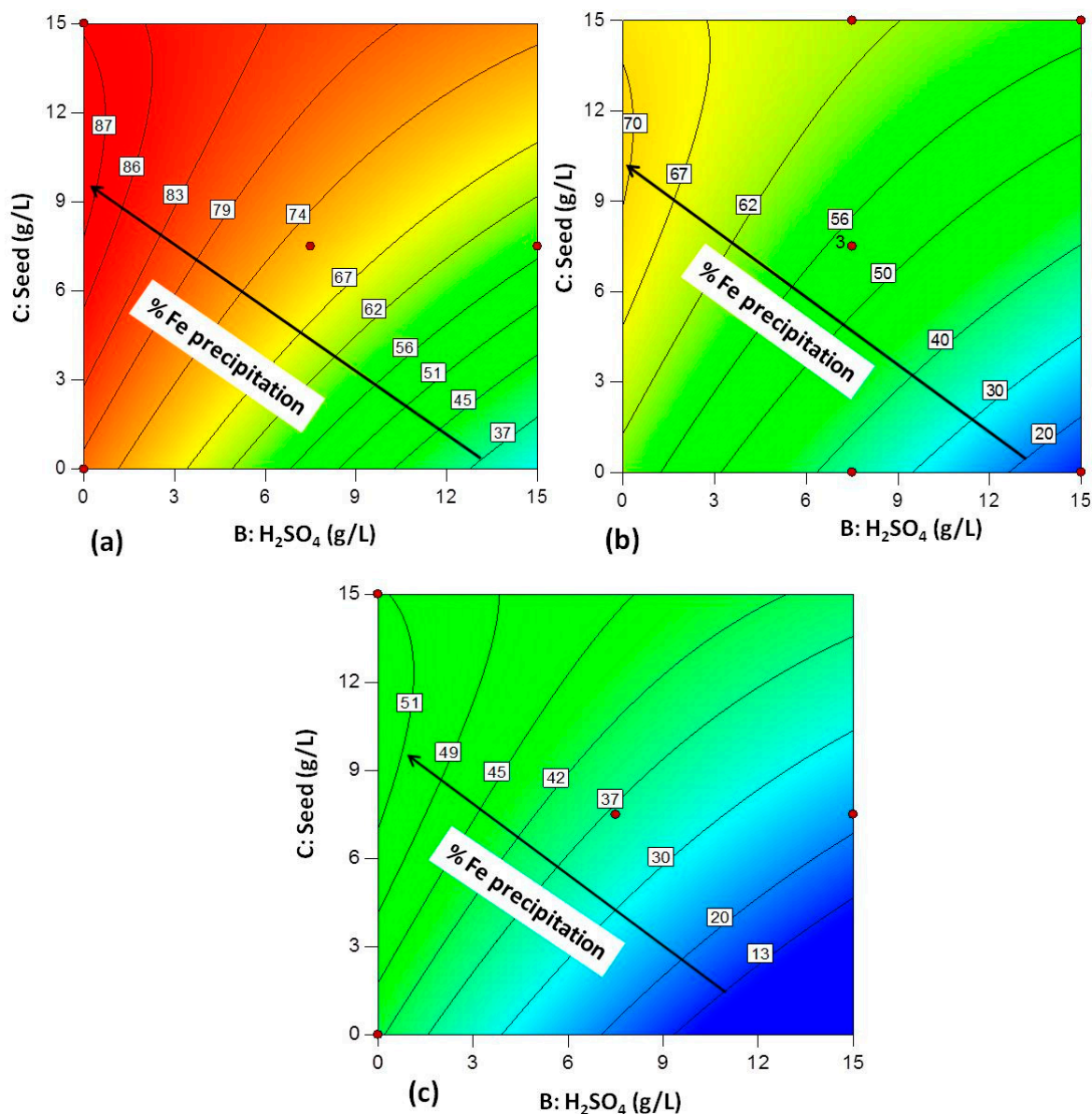


Figure 3. The 2D contour plots for the interaction effects of initial H_2SO_4 and seed concentrations on %Fe(III) precipitated: (a) Initial Fe(III) = 6 g/L, (b) initial Fe(III) = 10.5 g/L, (c) initial Fe(III) = 15 g/L.

Figure 4a shows that increasing acid concentration from 0 to 15 g/L decreased the Cu content of the precipitates from about 0.8% to about 0.4%. Figure 4b,c shows that addition of hematite seed further reduced the copper content of the precipitates. Comparison between Figure 4b,c shows that the difference between %Cu content of the precipitates for medium and high levels of seeding was not significant (even though the solids were diluted with a higher amount of seed, which did not take Cu). It was observed that seed itself did not result in copper loss in the absence of fresh precipitates. After necessary correction for the dilution effect of seed, the Cu/Fe ratios of the fresh precipitates are plotted in Figure 5. Figure 5a,b shows that presence of high acid, low ferric, and medium seeding generated the precipitates with the least amount of copper in the solids. However, high seed levels, as shown in Figure 5c, did not improve the Cu uptake of the precipitates significantly. For the same ferric concentration of solution, higher seeding levels provided more surface area for surface nucleation, which resulted in a decrease in the growth-to-nucleation ratio. XRD analysis of the precipitates for high seeding level detected two generations of hematite: One with well crystallized narrow peaks and the other nanoscale with broad, diffuse peaks. The more probable explanation seems that the

new nuclei were formed and some of the newly precipitated material was present as distinct separate particles. This could have been due to higher secondary nucleation, collisions, and energies, which resulted in more fine fractions in the product [42]. Claassen and Sandenbergh [43] also observed a similar effect for high seed levels in their system.

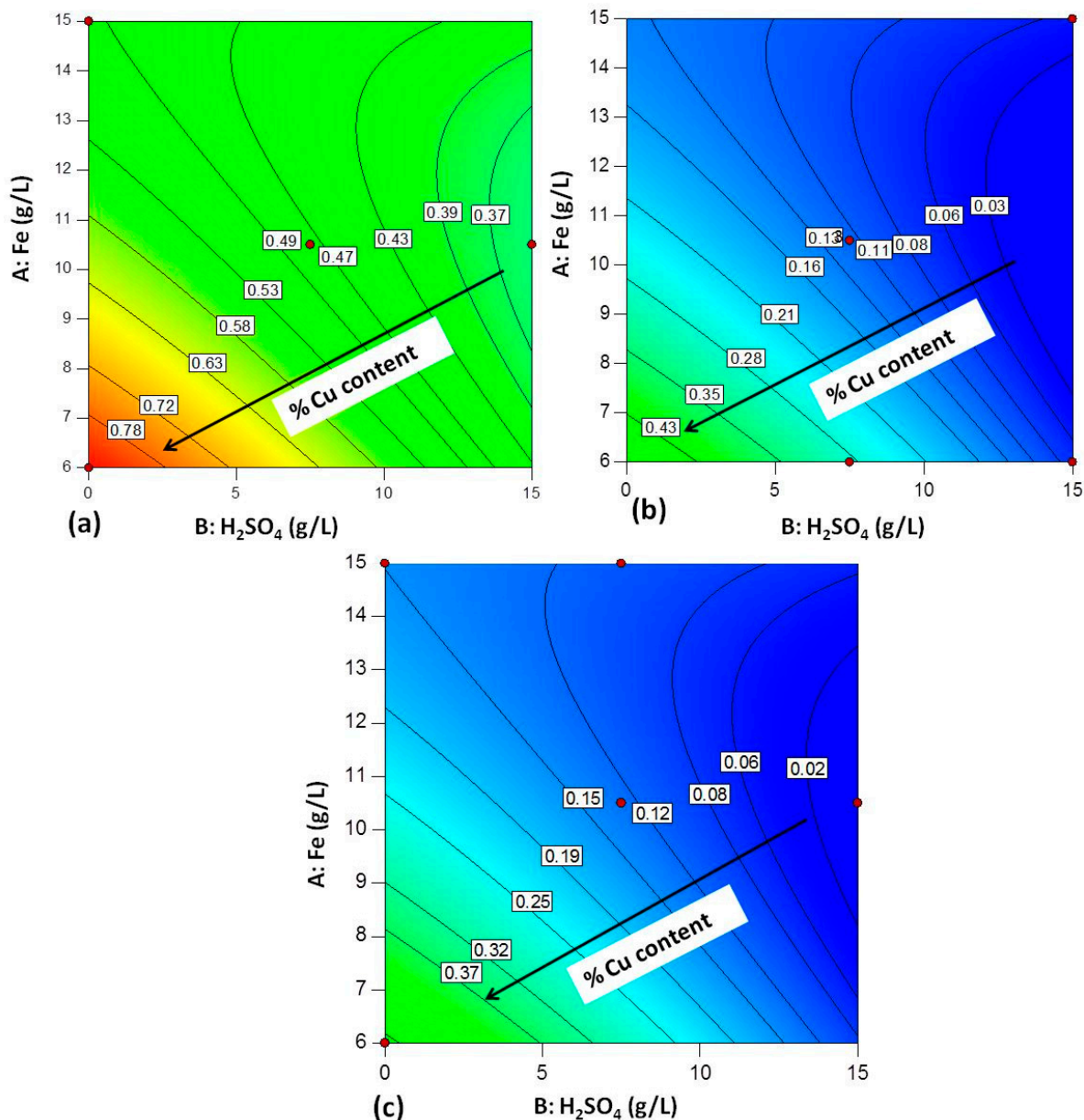


Figure 4. The 2D contour plots for the interaction effects of initial H₂SO₄ and initial Fe(III) concentrations on %Cu content of precipitates: (a) Seed = 0 g/L, (b) seed = 7.5 g/L, (c) seed = 15 g/L.

It was difficult in this study to differentiate the individual effect of the factor A due to the fact that more acid was generated at higher initial ferric concentrations, Equation (2), which was confounded with factor B. Therefore, instead of the individual term “A”, the interaction term “AB” became more important for %Cu content of the precipitates. A decrease in the copper content of the precipitates at higher acid concentrations, as seen in Figure 4a–c, was attributed to an increase in equilibrium ferric concentration of the solution, leading to a slower nucleation rate, which resulted in larger particles (see Figures 6 and 7) and relatively lower adsorption of divalent ions or solution occlusion. Ruiz et al. [23] also observed an increase in the particle size of precipitates at higher acid concentrations.

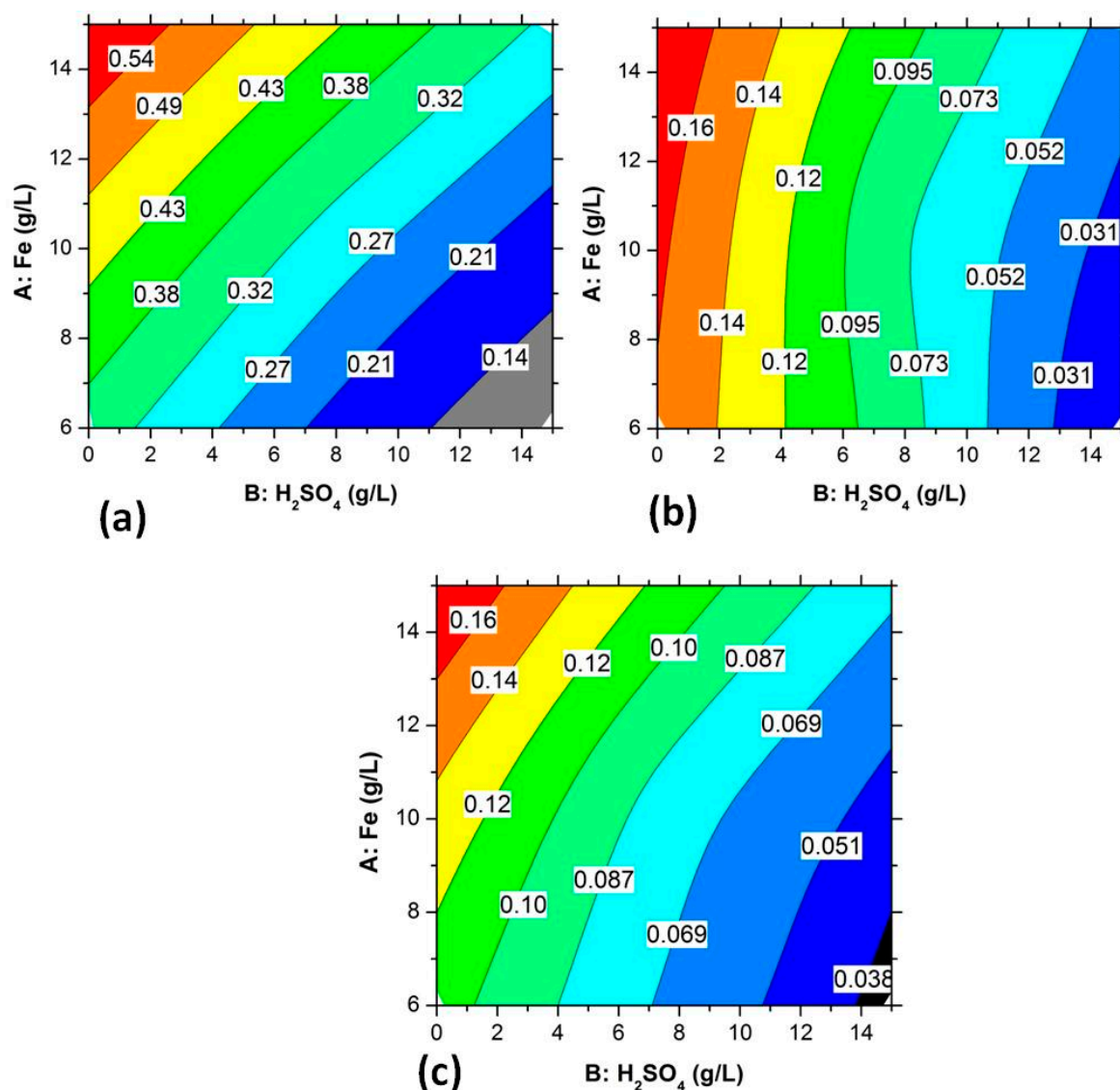


Figure 5. Cu/Fe ratio ($\%Cu/\%Fe \times 100$) of precipitates plotted for the interaction effects of initial H_2SO_4 and initial Fe(III) concentrations: (a) Seed = 0 g/L, (b) seed = 7.5 g/L, (c) seed = 15 g/L.

Table 8. Initial and final conditions of the solutions and mineral phases of the precipitates.

Experiment No.	Fe(III) (g/L)		Cu(II) (g/L)		Free Acid (g/L) ²		Mineral Phase Precipitated ¹
	Initial	Final	Initial	Final	Initial	Final	
F-1	15	6.2	30	29.3	0	22.7	H
F-2	15	4.0	30	28.8	0	29.2	H
F-3	15	13.1	30	29.8	15	19.1	H + V
F-4	15	7.3	30	29.5	15	34.5	H
F-5	6	5.0	30	29.8	15	17.6	H
F-6	6	0.58	30	29.9	0	14.6	H
F-7	6	0.29	30	29.7	0	15.2	H
F-8	6	1.0	30	29.7	15	27.9	H
G-1	6	2.3	30	29.8	15	24	H
G-2	15	9.6	30	29.5	7.5	21.3	H
G-3	6	1.6	30	29.5	7.5	20.3	H
G-4	15	11.5	30	28.9	15	24.2	H
G-5	15	7.9	30	27.5	0	18.2	H + V
G-6	10.5	9.4	30	29.6	15	18	H

Table 8. Cont.

Experiment No.	Fe(III) (g/L)		Cu(II) (g/L)		Free Acid (g/L) ²		Mineral Phase Precipitated ¹
	Initial	Final	Initial	Final	Initial	Final	
G-7	10.5	6.3	30	28.8	7.5	19.6	H
G-8	6	1.3	30	27.8	0	12.5	H + G
G-9	6	0.6	30	28.4	0	14.2	H
G-10	10.5	3.5	30	29.3	7.5	26.1	H
G-11	10.5	5.0	30	29.7	15	28.4	H
G-12	15	5.5	30	29.3	0	23.2	H
G-13	10.5	4.8	30	29.5	7.5	22.5	H
G-14	10.5	4.6	30	29.4	7.5	22.8	H
G-15	10.5	4.7	30	29.7	7.5	22.3	H

¹ H, Hematite; V, $\text{Fe}_4(\text{SO}_4)(\text{OH})_{10}$; G, goethite. ² Free acid was measured via titration as described in the experimental section.

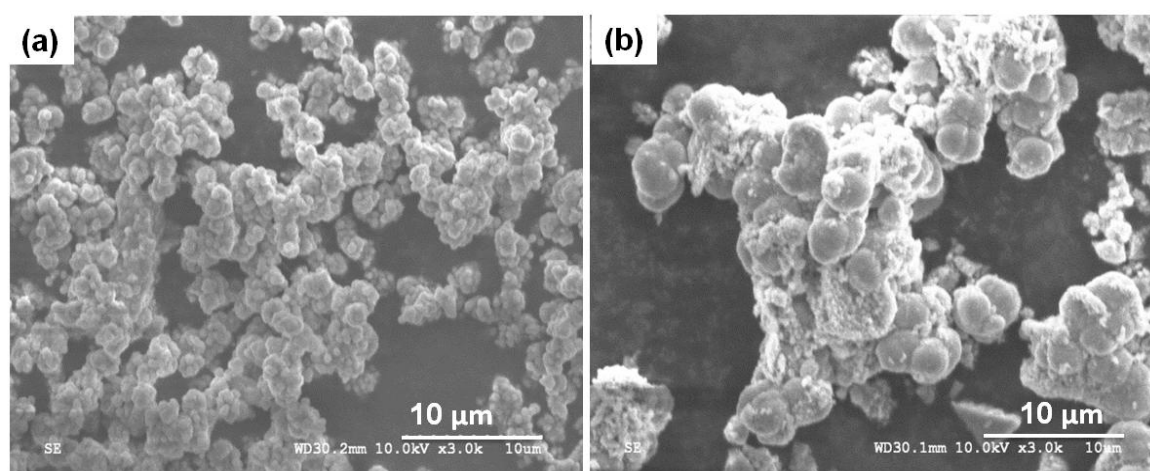


Figure 6. SEM images of the precipitates: (a) 0 g/L initial H_2SO_4 and (b) 15 g/L initial H_2SO_4 . Other conditions: 6 g/L Fe(III), 30 g/L Cu(II), 11g/L Cl^- , 1 h, 150 °C.

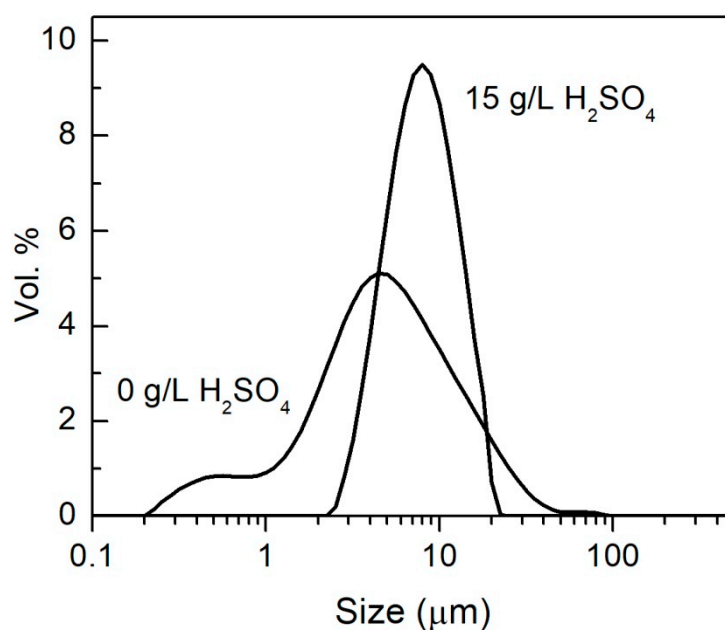


Figure 7. Particle size distribution of the precipitates: Other solution conditions: 6 g/L Fe(III), 30 g/L Cu(II), 11g/L Cl^- , 1 h, 150 °C.

5.3. Mechanism of Cu Loss to the Precipitates

Adsorption of Cu(II) onto hematite at relatively high pH values ($\text{pH} > \sim 2$) is well discussed in the literature [44–47]. Peacock and Sherman [45] described the adsorption of Cu(II) ion by considering surface complexes ($\text{Fe}-\text{O}^- + \text{Cu}^{2+} \rightarrow \text{Fe}-\text{OCu}^+$) on the hematite particles. Unpaired bonds at the surface of hematite create a localized electric field and electric potential further increases if the particles approach nanosize (typically < 7 nm) because of a decrease in the symmetry of the bonding environments on the smaller particles relative to the larger particles, resulting in relatively higher uptake of the cation [48]. However, Tombácz et al. [49] found that for lower pH values ($\text{pH} < \sim 2$), where the activity of the proton is high, protonation ($\text{Fe}-\text{O}^- + \text{H}^+ \rightarrow \text{Fe}-\text{OH} + \text{H}^+ \rightarrow \text{Fe}-\text{OH}_2^+$) of the surface sites of the hematite particles takes place. These positively charged protonated sites are complexed with negatively charged SO_4^{2-} in the solution. This mechanism leads to hematite with relatively higher sulphate and lower copper content. Charge reversal of the surface sites takes place when the SO_4^{2-} adsorption capacity of the hematite is reached, making the surface suitable for cation uptake. The competitive sorption of the Cu(II) and SO_4^{2-} on the hematite particles depend upon the concentration of the excess cations or anions in the solution.

On the other hand, substitution of Cu(II) into the hematite structure can serve as another means of copper loss to precipitates. Although Cu(II) and Fe(III) ions have a large difference in ionic radii (0.073 and 0.0645 nm, respectively) and can cause charge neutrality issues when replacing the other, in highly acidic environments Cu(II) can replace Fe(III). This is suggested to be due to the fact that charge balance is achieved by uptake of protons on the particle surface and an enlarged cell parameter “c” is observed due to the Jahn–Teller effect of copper ions in the hematite structure [50].

It is of further interest to study the exact mechanism of copper loss to the precipitates by using a combination of techniques such as: X-ray absorption fine structure spectroscopy (XAFS), XRD, and TEM.

6. Optimum Parameters

Figures 3 and 4 show that, in the absence of seed, if the target is set to achieve maximum “%Fe(III) Precipitated”, lower acid levels should be used, but if the target is to reduce the “%Cu Content” of the precipitates, higher acid levels will be favorable. Hence, both targets cannot be achieved at the same time. However, in the presence of moderate amounts of seed, Cu loss can be minimized with moderate to high iron precipitation levels from the acidic media. For example, Figures 3a and 4b show that, in the presence of 15 g/L initially added H_2SO_4 , 7.5 g/L seed and 6 g/L initial Fe(III), about 60% of the iron was precipitated with $< 0.1\%$ Cu content in the precipitates. However, under the same conditions but in the absence of seed about 35% iron was precipitated with about 0.45% Cu content of the precipitates, see Figures 3a and 4a. Similarly, Figure 5 shows that high acid and low ferric concentrations resulted in the lowest Cu/Fe ratios in the precipitates. The predicted models and contour plots suggest that a high acid and the presence of a moderate amount of seed produced the best results. The high acid environment created low supersaturation (because of higher equilibrium ferric solubility in acid) and resulted in a slower nucleation rate or preferred particle growth over nucleation, resulting in relatively coarser particles, see Figures 6 and 7. Demopoulos [40] and Claassen and Sandenbergh [43] have described the effect of supersaturation on particle growth and product quality.

7. Phase Analysis of the Precipitates

The precipitation products generated under different experimental conditions were analyzed by XRD and the mineral phases of the solid phases are given in Table 8. Hematite was the dominant phase in all cases. However, under certain experimental conditions, the precipitates contained certain amounts of either $\text{Fe}_4(\text{SO}_4)(\text{OH})_{10}$ (a compound having an XRD pattern virtually identical to volaschioite [51]) or goethite. The restriction of $\text{Fe}_4(\text{SO}_4)(\text{OH})_{10}$ to samples F-3 and G-5 and goethite to G-8 alone showed that the former is favored under high initial acid concentrations while the

latter is favored under low initial acid concentrations. The quantitative powder diffraction analysis of the precipitates showed the precipitates to consist of about 10–15% amorphous phase under all experimental conditions, except when retention time was ≥ 4 h or when hematite seed was present. For retention times ≥ 4 h, only hematite was detected by XRD. Therefore, the presence of amorphous phase was attributed to the short retention times generally used in this study. The higher sulphur content of the precipitates for shorter retention times suggested that the amorphous phase could be either basic ferric sulphate or schwertmannite or some other iron hydroxy-sulphate phase. Claassen et al. [9] found the amorphous phase to be schwertmannite in acidic sulphate medium. These authors used Mössbauer effect spectroscopy to confirm its presence. Identification of the exact nature of the intermediate metastable phase, in this study, needs further investigation.

8. Conclusions

The statistically designed experiments successfully identified the significant factors and their interactions affecting the “%Fe(III) precipitated” and “%Cu content of the solids”. The factors initial ferric and H_2SO_4 concentrations and their interactions were identified by fractional factorial design to be the important factors determining the “%Cu content” of the precipitates. However, the factors initial ferric, H_2SO_4 , retention time, and seed were important to determine the “%Fe(III) precipitated”. Initial ferric, H_2SO_4 and seed concentrations were further studied at three levels using a Box–Behnken design and the data were used to create contour plots. Mathematical models for “%Fe(III) precipitated” and “%Cu content of precipitates” were developed by fitting the data to a quadratic model. The predicted models were successful to explain the factors and their interactions which maximize “%Fe(III) precipitation” and minimize “%Cu content”. The predicted models can be used for the existing processes as well as for those in the development stages. However, care should be taken to use the predicted models and contour plots for the conditions outside of the range of conditions studied.

The results showed that the presence of high acid and moderate amount of seed were the more suitable conditions to minimize %Cu content of the solids while achieving moderate to high levels of %Fe(III) precipitation. The results also showed that the supersaturation and the nucleation-to-growth ratios determined the final product quality, i.e., the final particle size and Cu and SO_4^{2-} content of the precipitates. High acid concentrations created low supersaturation environment, which resulted in slower nucleation rate and preferred particle growth. Presence of a certain amount of seed was always beneficial. However, high seed levels resulted in more fine fractions in the product due to higher secondary nucleation, collisions, and energy in the system.

Author Contributions: Through the course of his doctoral studies, T.J. designed and carried out the experiments, analyzed the data, and wrote the initial draft of this paper. E.A. supervised the work, contributed to the experimental plan and data analysis, and edited the manuscript. All authors have read and agreed to the published version of the manuscript.

Funding: This research was funded by Teck, Vale, and the Natural Science and Engineering Research Council (NSERC) of Canada, through grant # CRDPJ 436614-12.

Acknowledgments: The authors are thankful to Henry Salomon-de-Friedberg, Superintendent of New Technologies at CESL Ltd., and Indje Mihaylov, Section Head Hydrometallurgy, Vale Technical Services Limited, for many useful discussions, ideas, and support of the research. The authors also wish to acknowledge Matti Raudsepp, for his support with XRD measurements throughout this research program.

Conflicts of Interest: The authors report no conflict of interest.

Appendix A

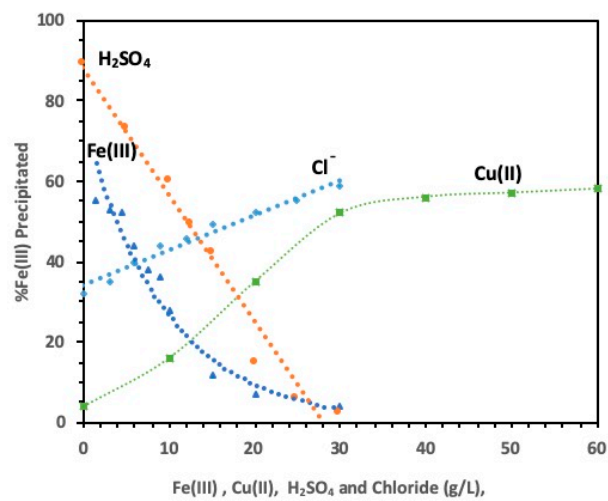


Figure A1. Effect of initial Fe(III), H₂SO₄, Cu(II), and chloride on %Fe(III) precipitation at 150 °C for 1 h. Fe(III) line: 15 g/L H₂SO₄, 11 g/L Cl⁻, 30 g/L Cu(II). H₂SO₄ line: 6 g/L Fe(III), 11 g/L Cl⁻, 30 g/L Cu(II). Cl⁻ line: 6 g/L Fe(III), 15 g/L H₂SO₄, 30 g/L Cu(II). Cu(II) line: 6 g/L Fe(III), 15 g/L H₂SO₄, 11 g/L Cl⁻. Data extracted and replotted from [26].

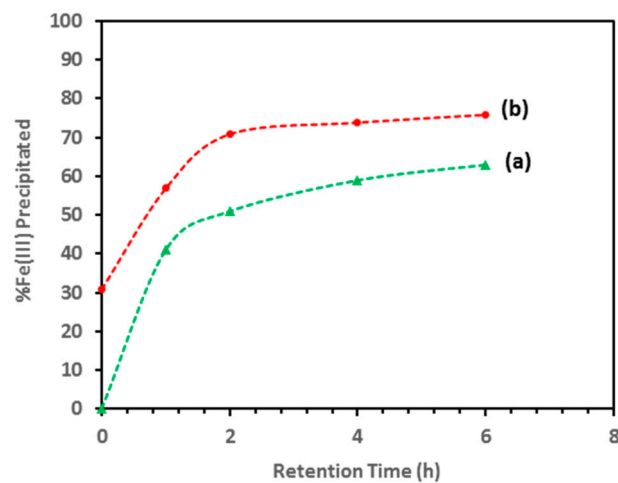


Figure A2. Effect of retention time on Fe(III) precipitation from solutions containing 6 g/L Fe(III), 15 g/L H₂SO₄, 11 g/L Cl⁻, and 30 g/L Cu(II) at 150 °C; (a) 0.0 g/L seed; (b) 15.0 g/L hematite seed. Data replotted from [26].

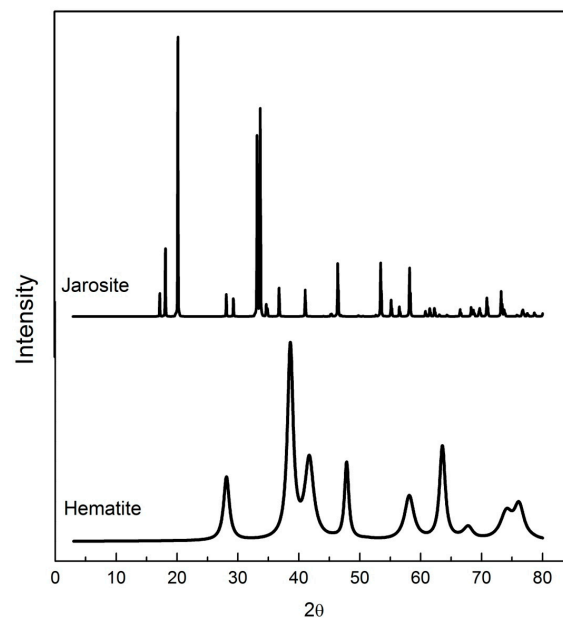


Figure A3. Calculated XRD patterns of hematite and jarosite formed in the experiments. Hematite was the dominant phase for initial ferric levels <15 g/L Fe(III) while jarosite was favored at ferric concentrations >15 g/L Fe(III). Actual collected patterns for these minerals are shown in Figures A4 and A5.

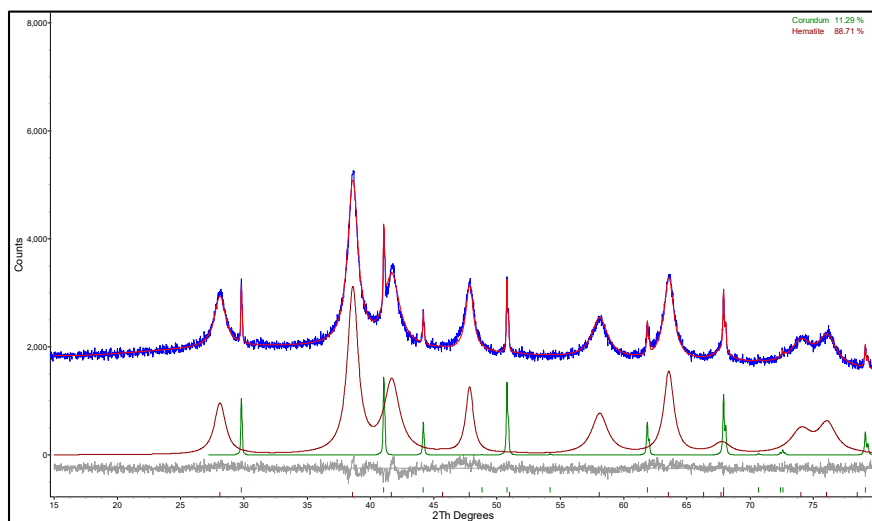


Figure A4. Rietveld refinement plot of sample containing hematite (blue line—observed intensity at each step; red line—calculated pattern; solid grey line, below, difference between observed and calculated intensities; green line corundum standard added for quantification; vertical bars, positions of all Bragg reflections).

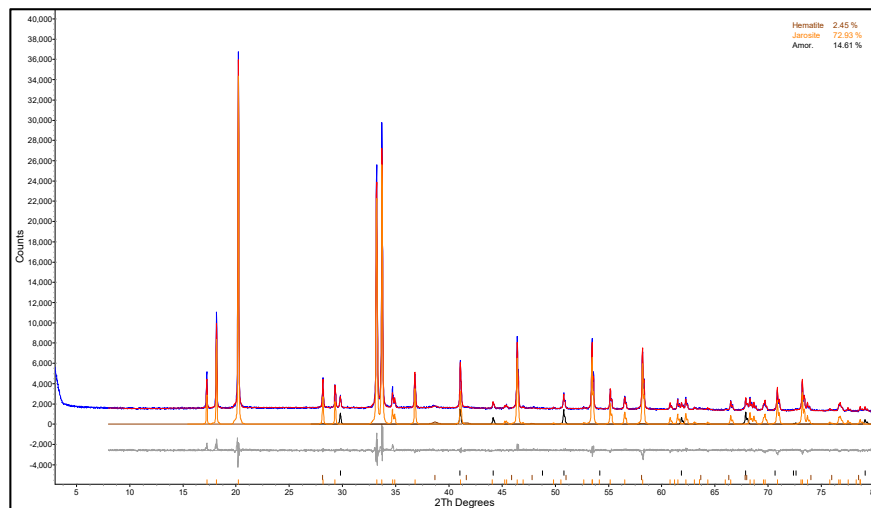


Figure A5. Rietveld refinement plot of sample containing jarosite as the major phase (blue line—observed intensity at each step; red line—calculated pattern; solid grey line, below, difference between observed and calculated intensities; vertical bars, positions of all Bragg reflections).

Appendix B. Box–Behnken Design

The Box-Behnken design is an independent quadratic design to navigate response surfaces. The treatment combinations are at the midpoints of the edges of the process space and at the center (i.e., midpoints of the edges of a cube and its center). These designs are rotatable (or near rotatable) and require three levels of each factor. The number of experiments in this design were $N = 2k(k - 1) + C_0$, where, k is the number of factors and C_0 is the number of central points. The experimental data were normally fitted to a quadratic model, given below:

$$Y = \beta_0 + \sum_{i=1}^k \beta_i x_i + \sum_{i=1}^k \sum_{j=1}^k \beta_{ij} x_{ij} + \sum_{i=1}^k \beta_{ii} x_{ii}^2 + \varepsilon, \quad (\text{A1})$$

where Y is the response variable, β_0 is regression coefficient, β_i is linear coefficient. and β_{ij} , β_{ii} are coefficients of the quadratic terms. The term ' ε ' represents the random errors. The error terms, in general, were normally distributed. The relationship between the coded and actual factors can be written as:

$$x_i = \frac{X_i - X_0}{\Delta X} \quad (\text{A2})$$

where X_i is the actual value of the variable, x_i is the coded value, X_0 is the actual value of the variable at the central point, and ΔX corresponds to the unit variation of the value.

Appendix C. Transformation Applied to %Fe(III) Precipitated in Figure 1

Often response variables are normalized by applying power transformations, from the family $y^* = y^\lambda$, where λ is parameter of the transformation to be determined (e.g., $\lambda = -1/2$ means use the inverse square root of the original response). This procedure uses the method of maximum likelihood. Various values of λ are selected and a standard analysis of variance is performed on:

$$y^{(\lambda)} = \frac{y^{\lambda-1}}{\lambda \dot{y}^{\lambda-1}}, \quad y^{(0)} = \dot{y} \ln y, \quad (\text{A3})$$

The value of $\lambda = 0$ corresponds to the log transformation and it can be shown that $y^{(0)} = \dot{y} \ln y$. The quantity \dot{y} is the geometric mean of the response data. The maximum likelihood value for λ , for the fitted model, is the lowest point in the graph of residual sum of squares (RSS) versus λ [29],

as shown in Figure A6. For the %Fe(III) precipitated used in this study, values of ($\ln RSS$) for various values of λ are plotted in Figure A6, according to the guidelines provided by the software package (Design-Expert®). The values ($\ln RSS$) are used because the range of values for (RSS) is quite large. An approximate 95% confidence interval for (λ) may also be obtained from the graph by calculating the critical sum of squares (SS^*):

$$SS^* = RSS \left[1 + \frac{t_v^2(0.025)}{\nu} \right], \quad (A4)$$

where ν is the number of degrees of freedom. A line is plotted parallel to λ -axis at a height SS^* on the graph of ($\ln RSS$) versus λ . By locating the points on λ -axis where the SS^* cuts the curve ($\ln RSS$), we can read the 95% confidence interval limits on λ directly from the graph. The values of low and high confidence interval in this study were -0.3 and 0.91 , respectively. The optimum value of λ in this case was 0.18 , which is the lowest point in the ($\ln RSS$) versus λ graph. As the minimum value of λ and zero both fall within the 95% confidence limit, therefore, the transformation procedure was good enough to process the %Fe(III) precipitation in Figure A6.

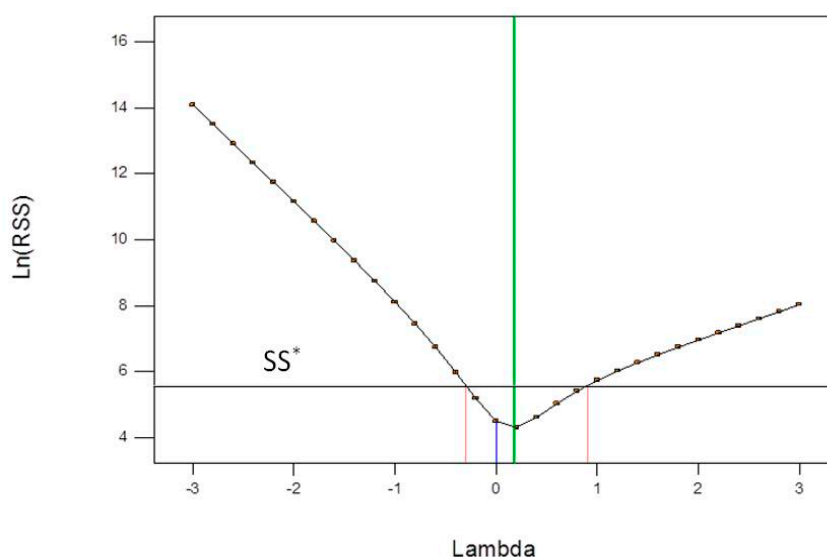


Figure A6. Box–Cox plot for the power transformation applied to %Fe(III) precipitation.

References

1. Beaulieu, R.; Gagne, G.; Nasmyth, M.; Cooper, G.; Inostroza, C. Iron Control and Management in the Zinc Industry. In *Iron Control Technologies: Proceedings of the Third International Symposium on Iron Control in Hydrometallurgy, Montreal, QC, Canada, 1–4 October 2006*; Dutrizac, J.E., Riveros, P.A., Eds.; Canadian Institute of Mining, Metallurgy and Petroleum: Montreal, QC, Canada, 2006; pp. 45–55.
2. Hackl, R.P.; Dreisinger, D.B.; Peters, E.; King, J. Passivation of chalcopyrite during oxidative leaching in sulfate media. *Hydrometallurgy* **1995**, *39*, 25–48. [[CrossRef](#)]
3. Tainton, U.C.; Lyeson, L.T. Electrolytic zinc from complex ores. *Trans. Am. Inst. Min. Metall. Pet. Eng.* **1924**, *70*, 486–522.
4. Dutrizac, J.E. An overview of iron precipitation in hydrometallurgy. In *Crystallization and Precipitation*; Strathdee, G.L., Klein, M.O., Melis, L.A., Eds.; Pergamon Press: Saskatoon, SK, Canada, 1987; pp. 259–283.
5. Schwertmann, U.; Friedl, J.; Stanjek, H. From Fe (III) ions to ferrihydrite and then to hematite. *J. Colloid Interface Sci.* **1999**, *209*, 215–223. [[CrossRef](#)]
6. Cornell, R.M.; Giovanoli, R.; Schneider, W. Review of hydrolysis of iron (III) and the crystallisation of amorphous iron (III) hydroxide hydrate. *J. Chem. Technol. Biotechnol.* **1989**, *46*, 115–134. [[CrossRef](#)]
7. Das, S.; Hendry, M.J.; Essilfie-Dughan, J. Transformation of two-line ferrihydrite to goethite and hematite as a function of pH and temperature. *Environ. Sci. Technol.* **2011**, *45*, 268–275. [[CrossRef](#)] [[PubMed](#)]

8. Žic, M.; Ristić, M.; Musić, S. Monitoring the hydrothermal precipitation of α -Fe₂O₃ from concentrated Fe(NO₃)₃ solutions partially neutralized with NaOH. *J. Mol. Struct.* **2011**, *993*, 115–119. [[CrossRef](#)]
9. Claassen, J.O.; Meyer, E.H.O.; Rennie, J.; Sandenbergh, R.F. Iron precipitation from zinc-rich solutions: Defining the Zincor Process. *Hydrometallurgy* **2002**, *67*, 87–108. [[CrossRef](#)]
10. Loan, M.; Newman, O.G.M.; Cooper, R.M.G.; Farrow, J.B.; Parkinson, G.M. Defining the paragoethite process for iron removal in zinc. *Hydrometallurgy* **2006**, *81*, 104–129. [[CrossRef](#)]
11. Javed, T.; Abdul, B.; Ryan, D.; Raudsepp, M.; Asselin, E. Amorphous iron phases in medium temperature leach residues and associated metal loss. *Int. J. Miner. Process.* **2016**, *148*, 65–71. [[CrossRef](#)]
12. Dyer, L.; Su, B.; Asselin, E. Cobalt loss due to iron precipitation in ammoniacal carbonate solutions. *Hydrometallurgy* **2012**, *125–126*, 144–147. [[CrossRef](#)]
13. Sahu, S.K.; Asselin, E. Characterization of residue generated during medium temperature leaching of chalcopyrite concentrate under CESL conditions. *Hydrometallurgy* **2011**, *110*, 107–114. [[CrossRef](#)]
14. Steel, A.; Hawboldt, K.; Khan, F. Assessment of minerals and iron-bearing phases present in hydrometallurgical residues from a nickel sulfide concentrate and availability of residue associated metals. *Hydrometallurgy* **2010**, *101*, 126–134. [[CrossRef](#)]
15. Loan, M.; Parkinson, G.M.; Newman, M.; Farrow, J.B. Iron oxy-hydroxide crystallization in a hydrometallurgical residue. *J. Cryst. Growth* **2002**, *235*, 482–488. [[CrossRef](#)]
16. Loan, M.; Richmond, W.R.; Parkinson, G.M. On the crystal growth of nanoscale schwertmannite. *J. Cryst. Growth* **2005**, *275*, 1875–1881. [[CrossRef](#)]
17. Bigham, J.M.; Carlson, L.; Murad, E. Schwertmannite, a new iron oxyhydroxysulfate from Pyhlsalmi, Finland, and other localities. *Miner. Mag.* **1994**, *58*, 641–648. [[CrossRef](#)]
18. Claassen, J.O.; Sandenbergh, R.F. Influence of temperature and pH on the quality of metastable iron phases produced in zinc-rich solutions. *Hydrometallurgy* **2007**, *86*, 178–190. [[CrossRef](#)]
19. Loan, M.; Pierre, T.G.S.; Parkinson, M.; Newman, O.; Farrow, J. Identifying Nanoscale Ferrihydrite in Hydrometallurgical Residues. *JOM* **2002**, *54*, 40–43. [[CrossRef](#)]
20. Riveros, P.A.; Dutrizac, J.E. The precipitation of hematite from ferric chloride media. *Hydrometallurgy* **1997**, *46*, 85–104. [[CrossRef](#)]
21. Dutrizac, J.E.; Riveros, P.A. The Precipitation of Hematite from Ferric Chloride Media at Atmospheric Pressure. *Metall. Mater. Trans. B* **1999**, *30*, 993–1001. [[CrossRef](#)]
22. Umetsu, Y.; Tozawa, K.; Sasaki, K. The hydrolysis of ferric sulphate solutions at elevated temperatures. *Can. Metall. Q.* **1977**, *16*, 111–117. [[CrossRef](#)]
23. Ruiz, M.C.; Zapata, J.; Padilla, R. Effect of Variables on the Quality of Hematite Precipitated from Sulfate Solutions. *Hydrometallurgy* **2007**, *89*, 32–39. [[CrossRef](#)]
24. Dutrizac, J.E.; Chen, T.T. Factors Affecting the Precipitation of Hematite Rather than Jarosite in Nickel Sulphate-Chloride Solutions. In *Proceedings of Hydrometallurgy of Nickel and Cobalt*; Budac, J.J., Ed.; The Canadian Institute of Mining, Metallurgy and Petroleum: Montreal, QC, Canada, 2009; pp. 295–319.
25. Dutrizac, J.E.; Chen, T.T. Precipitation of Hematite Directly from Ferric Sulphate Solutions. *World Metall.* **2011**, *64*, 134–150.
26. Javed, T.; Xie, M.; Asselin, E. Factors affecting hematite precipitation and characterization of the product from simulated sulphate-chloride solutions at 150 °C. *J. Hydrometall.* **2018**, *179*, 8–19. [[CrossRef](#)]
27. Barr, G.; Defreyne, J.; Mayhew, K. *CESL Process—An Economic Alternative to Smelting*; CESL Ltd: Peterborough, UK, 2005.
28. Oehlert, G.W. *A First Course in Design and Analysis of Experiments*; W.H. Freeman: New York, NY, USA, 2000.
29. Wang, K.; Li, J.; McDonald, R.G.; Browner, R.E. The effect of iron precipitation upon nickel losses from synthetic atmospheric nickel laterite leach solutions: Statistical analysis and modelling. *Hydrometallurgy* **2011**, *109*, 140–152. [[CrossRef](#)]
30. Box, G.E.P.; Hunter, W.G.; Hunter, J.S. *Statistics for Experiments: An Introduction to Design, Data Analysis, and Model Building*; John Wiley and Sons, Inc.: New York, NY, USA, 1978.
31. Myers, R.H.; Montgomery, D.C. *Response Surface Methodology: Process and Product Optimization Using Designed Experiments*; John Wiley and Sons, Inc.: New York, NY, USA, 2002.
32. Burkin, A.R. Use of Statistical Methods of Experimental Design in Optimizing Hydrometallurgical Processes. *Hydrometall. Process Fundam.* **1984**, *10*, 529–538.

33. Agatzini, S.; Burkin, A.R. Statistical approach to the precipitation of iron as 'goethite'. *Trans. Inst. Min. Metall. Sect.* **1985**, *94*, C105–C114.
34. De La Torre, A.G.; Bruque, S.; Aranda, M.A.G. Rietveld quantitative amorphous content analysis. *J. Appl. Crystallogr.* **2001**, *34*, 196–202. [[CrossRef](#)]
35. Rolia, E.; Dutrizac, J.E. The Determination of Free Acid in Zinc Processing Solutions. *Can. Metall. Q.* **1984**, *23*, 159–167. [[CrossRef](#)]
36. Jones, D.L.; Mayhew, K.; Connor, L.O. Nickel and cobalt recovery from a bulk copper-nickel concentrate using the CESL process. In *Hydrometallurgy of Nickel and Cobalt*; Budac, J.J., Fraser, R., Mihaylov, I., Eds.; CIM: Montreal, QC, Canada, 2009; pp. 45–58.
37. Box, G.E.P.; Behnken, D.W. Some new three level designs for the study of quantitative variables. *Technometrics* **1960**, *2*, 455–475. [[CrossRef](#)]
38. Daniel, C. Use of half-normal plots in interpreting factorial two-level experiments. *Technometrics* **1959**, *1*, 311–341. [[CrossRef](#)]
39. Box, G.E.P.; Cox, D.R. An analysis of transformations. *J. R. Stat. Soc.* **1964**, *26*, 211–246. [[CrossRef](#)]
40. Demopoulos, G.P. Aqueous precipitation and crystallization for the production of particulate solids with desired properties. *Hydrometallurgy* **2009**, *96*, 199–214. [[CrossRef](#)]
41. Daniel, C. *Applications of Statistics to Industrial Experimentations*; John Wiley and Sons, Inc.: New York, NY, USA, 1976.
42. Dirksen, J.A.; Ring, T.A. Fundamentals of crystallization: Kinetic effects on particle size distributions and morphology. *Chem. Eng. Sci.* **1991**, *46*, 2389–2427. [[CrossRef](#)]
43. Claassen, J.O.; Sandenbergh, R.F. Particle growth parameters in the precipitation of metastable iron phases from zinc-rich solutions. *Hydrometallurgy* **2006**, *84*, 165–174. [[CrossRef](#)]
44. Rose, A.W.; Bianchi-Mosquera, G.C. Adsorption of Cu, Pb, Zn, Co, Ni, and Ag on goethite and hematite: A control on metal mobilization from red beds into stratiform copper deposits. *Econ. Geol.* **1993**, *88*, 1226–1236. [[CrossRef](#)]
45. Peacock, C.L.; Sherman, D.M. Copper(II) sorption onto goethite, hematite and lepidocrocite: A surface complexation model based on ab initio molecular geometries and EXAFS spectroscopy. *Geochim. Cosmochim. Acta* **2004**, *68*, 2623–2637. [[CrossRef](#)]
46. Chen, Y.H.; Li, F.A. Kinetic Study on Removal of Copper (II) Using Goethite and Hematite Nano-Photocatalysts. *J. Colloid Interface Sci.* **2010**, *347*, 277–281. [[CrossRef](#)]
47. Grover, V.A.; Hu, J.; Engates, K.E.; Shipley, H.J. Adsorption and desorption of bivalent metals to hematite nanoparticles. *Environ. Toxicol. Chem.* **2012**, *31*, 86–92. [[CrossRef](#)]
48. Madden, A.S.; Hochella, M.F.; Luxton, T.P. Insights for size-dependent reactivity of hematite nanomineral surfaces through Cu²⁺ sorption. *Geochim. Cosmochim. Acta* **2006**, *70*, 4095–4104. [[CrossRef](#)]
49. Tombácz, E.; Libor, Z.; Illés, E.; Majzik, A.; Klumpp, E. The role of reactive surface sites and complexation by humic acids in the interaction of clay mineral and iron oxide particles. *Org. Geochem.* **2004**, *35*, 257–267. [[CrossRef](#)]
50. Cornell, R.M.; Schwertman, U. *The Iron Oxides: Structure, Properties, Reactions, Occurrences and Uses*, 2nd ed.; Wiley-VCH: Weinheim, Germany, 2003.
51. Biagioni, C.; Bonaccorsi, E.; Orlandi, P. Volaschioite, Fe₄(SO₄)O₂(OH)₆·2H₂O, a new mineral species from Forno Volaschio, Apuan Alps Tuscany, Italy. *Can. Mineral.* **2011**, *49*, 605–614. [[CrossRef](#)]

